

# Reshaping Particles by Collisions with Rigid Objects

Shiva Shahrokhi, Haoran Zhao, and Aaron T. Becker

**Abstract**— Consider many particles actuated by a global external field (e.g. gravitational or magnetic fields). In the absence of workspace obstacles, it is not possible to change the relative position of particles. Shape control of many particles is necessary for conveying information, construction, and for navigation. This paper presents analytical results using workspace obstacles and global inputs to reshape a group of particles. First we show how the particles' characteristic angle of repose can be used to reshape the particles by controlling angle of attack and the magnitude of the driving force. These can then be used to control the force and torque applied to a rectangular rigid body. Next, we examine the full set of stable achievable first and second moments for the shape of a particle group in two canonical environments: a square and a circular workspace. Then we show how workspaces with linear boundary layers can be used to achieve a more rich set of first and second moments. We conclude with hardware experiments investigating shape control using angle of repose and hardware boundaries.

## I. INTRODUCTION

**TODO:** lets do some experiments with salt in 3D printed shapes (or laser cut). Salt is micro scale, and roughly uniform (I think) we can get different magnitudes of global force by varying the tilt angle.

**TODO:** this text is from a previous paper

Particle swarms propelled by a uniform field, where each particle receives the same control input, are common in applied mathematics, biology, and computer graphics [1]–[3].

The small size of these robots makes it difficult to perform onboard computation. Instead, these robots are often controlled by a broadcast signal. The tiny robots themselves are often just rigid bodies, and it may be more accurate to define the robot as the *system* that consists of particles, a uniform control field, and sensing. Such systems are severely underactuated, having 2 degrees of freedom in the shared planar control input, but  $2n$  degrees of freedom for the  $n$ -particle swarm. Techniques are needed that can handle this underactuation.

Positioning is a foundational capability for a robotic system, e.g. placement of brachytherapy seeds. In previous work, we provided position control algorithms that only require non-slip wall contacts to position two robots [4]. We assumed that particles in contact with the boundaries have zero velocity if the uniform control input pushes the particle into the wall. This work analyses interactions between the boundary and the particle swarm to control shape of the

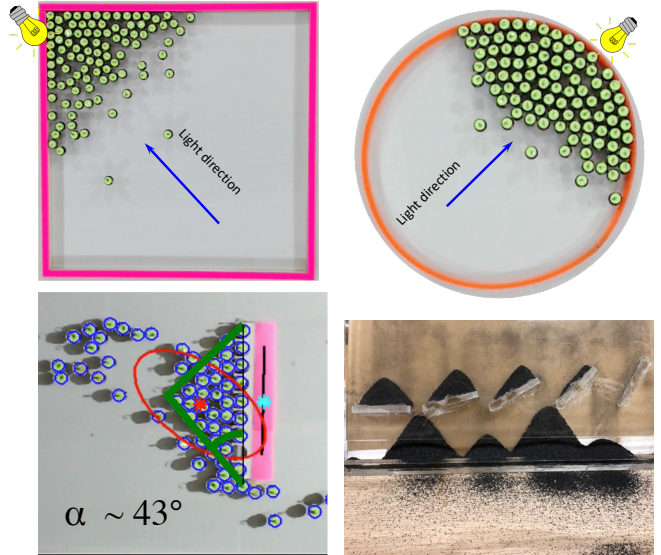


Fig. 1. Reshaping particles by collisions with rigid bodies. Top pictures illustrates using closed boundaries to reshape the particles. Bottom pictures illustrates angle of repose of different particles.

swarm. In [5] we showed how to control swarm statistics including mean position and variance. This work extends that work to covariance control.

The paper is arranged as follows. After a review of recent related work in Sec. II, Sec. III introduces angle of repose, a parameter of the particle swarm that can be used for shape control. Section IV describes implementations of the algorithms of covariance control in simulation and hardware experiments. We end with directions for future research in Sec. VI.

## II. RELATED WORK

Controlling the *shape*, or relative positions, of a swarm of robots is a key ability for a range of applications. Correspondingly, it has been studied from a control-theoretic perspective in both centralized and decentralized approaches. For examples of each, see the centralized virtual leaders in [6], and the gradient-based decentralized controllers using control-Lyapunov functions in [7]. However, these approaches assume a level of intelligence and autonomy in individual robots that exceeds the capabilities of many systems, including current micro- and nano-robots. Current micro- and nano-robots, such as those in [8]–[10] lack onboard computation.

\*This work was supported by the National Science Foundation under Grant No. [IIS-1553063] and [IIS-1619278].

Authors are with the Department of Electrical and Computer Engineering, University of Houston, Houston, TX 77204 USA  
{sshahrokhi2,atbecker}@uh.edu

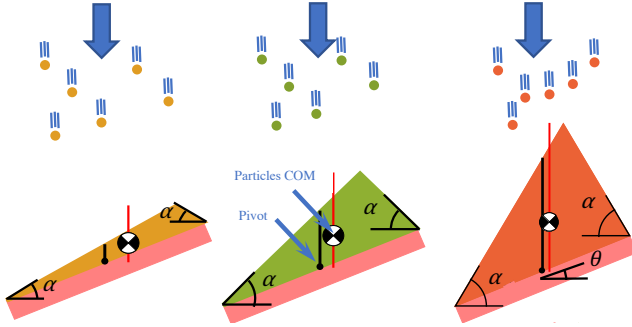


Fig. 2. If particles move faster than the (pink) rod, some particles slide past the rod, but the ones that remain pile up in a shape characterized by the angle of repose  $\alpha$ , which is particular to the particle type.

This paper focuses on centralized techniques that apply the same control input to both particles. Precision control requires breaking the symmetry caused by the uniform input. Symmetry can be broken using particles that respond differently to the uniform control signal, either through agent-agent reactions [11], or engineered inhomogeneity [12]–[14]. The magnetic gradients of MRI scanners are *uniform*, meaning the same force is applied everywhere in the workspace [15]. This work assumes a uniform control with homogenous particles, as in [16], and breaks the control symmetry using obstacles in the workspace.

Alternative techniques rely on non-uniform inputs, such as artificial force-fields. Applications have included techniques to design shear forces for sensorless manipulation of a single object by [17]. [18] demonstrated a collection of 2D force fields generated by six degree-of-freedom vibration inputs to a rigid plate. These force fields, including shear forces, could be used as a set of primitives for motion control to steer the formation of multiple objects.

Similarly, much recent work in magnet control has focused on exploiting inhomogeneities in the magnetic field to control multiple micro particles using gradient-based pulling [19], [20]. Unfortunately, using large-scale external magnetic fields makes it challenging to independently control more than one microrobot unless the distance between the electromagnetic coils is at the same length scales as the robot workspace [19]–[21]. In contrast, this paper requires only a controllable constant gradient in orthogonal directions to position the particles.

### III. ANGLE OF REPOSE

Consider a swarm of granular particles applying force to a rod. If the rod moves slower than the particles, some particles will slide past the rod, but other particles will build up behind the rod in a characteristic triangular shape defined by a steepest angle of descent perpendicular to the direction of particle motion. This piling up is common to all granular media, and the angle formed is a function of the *angle of repose*. Three different values of angle of repose is shown in Fig. 2. The center of mass of the rod is in the middle of the rod, but center of mass of the granular particles changes for

different values of angle of repose. By measuring the angle of repose for the particles shown in the top plot of Fig. 3, we can estimate the force and torque that the swarm is applying to the rod as a function of the rod's length, the angle of repose, and orientation of the rod. In this plot, particulate is moving in the  $-y$  direction, and the rods are tilted at  $\theta = \{-45, -22.5, 0, 22.5, 45\}^\circ$  with respect to the  $x$  axis. A thin black line extends upwards from the rod COM, and the COM of the particulate is shown by a white and black disk. More particulate is heaped on the right side of the rod for positive  $\theta$  and more on the left side for negative  $\theta$ . This uneven particulate generates a restoring torque. We define the angle of repose as  $\alpha$ , the rod's orientation relative to  $90^\circ$  from the particle movement vector as  $\theta$ , and the rod's length as  $\ell$ .

#### A. Force and Torque

By integrating over the triangular shape, the force applied to the rod (when a unit area of particles produces 1 N of force) is

$$F(\theta, \alpha, \ell) = \begin{cases} \frac{\ell^2 (\cos(2\theta) - \cos(2\alpha))}{8 \cos(\alpha) \sin(\theta)} & -\alpha < \theta < \alpha \\ 0 & \text{otherwise} . \end{cases} \quad (1)$$

The force for different angle of repose values are shown in the middle plot of Fig. 3, with the rod length  $\ell = 1$ . Torque will also be similarly defined as

$$\tau(\theta, \alpha, \ell) = \begin{cases} \frac{\ell^3 (\cos(2\alpha) - \cos(2\theta)) \sin(\theta)}{48 \sin^2(\alpha)} & -\alpha < \theta < \alpha \\ 0 & \text{otherwise} . \end{cases} \quad (2)$$

Torque is shown in the bottom plot of Fig. 3 with the rod length  $\ell = 1$ . Given sufficient particles to pile up to the angle of repose, this torque tends to stabilize the object to be perpendicular to the pushing direction. Force is maximized with  $\theta = 0$ , but the  $\theta$  value that maximizes torque is a function of  $\alpha$  and is defined as

$$\theta_{t_{\max}} = \frac{\sin(\alpha)}{\sqrt{3}} . \quad (3)$$

To maximize the torque a particulate swarm applies on a thin rod, the swarm should move in the direction  $-\theta_{t_{\max}} - 90^\circ$  with respect to the long axis of the rod.

#### B. Shape Control

Often the angle of the rigid rod is given, but we can choose the desired approach direction  $\beta$ . This section examines the possible shapes that can be generated given a rigid rod of length  $\ell$ , an angle of repose  $\alpha$ , and an approach angle where the swarm moves at angle relative to the long axis of the rod  $\beta$ .

Computing means, variances, covariance, and correlation requires integrating over  $R$ , the region containing the swarm

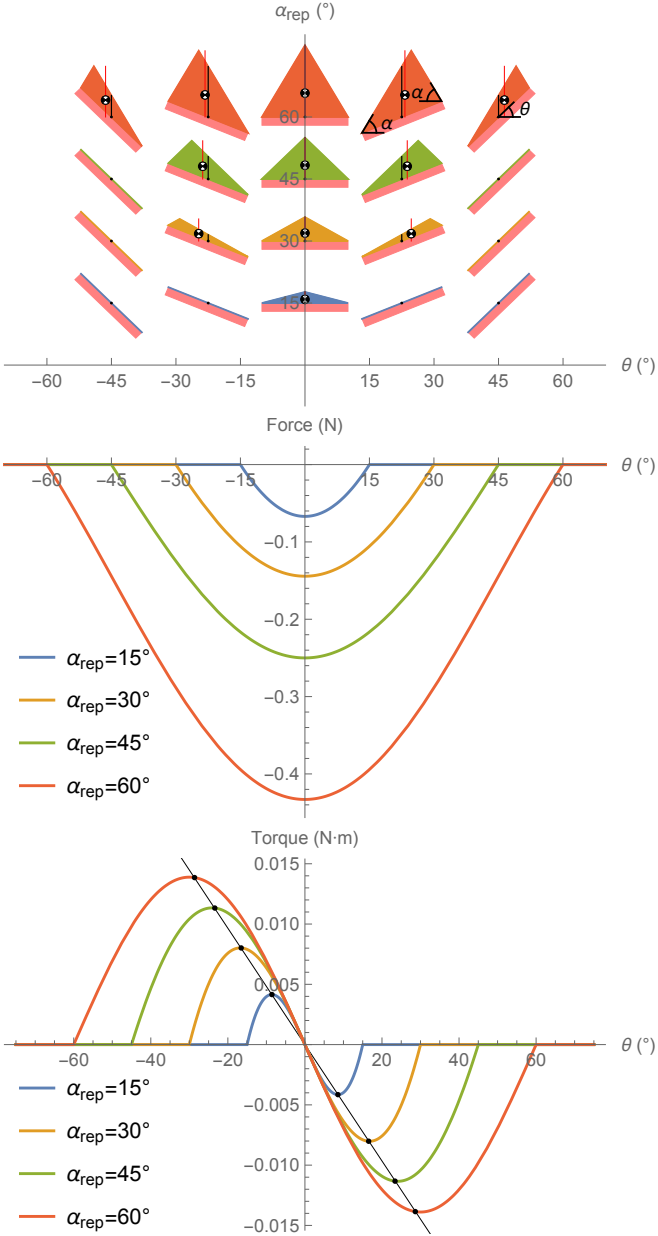


Fig. 3. Top plot shows colored particulate heaped up on pink-colored rods. Middle plot shows the force applied to the rod and bottom the torque as a function of  $\theta$  for four angle of repose values. The maximum torque values from (3) are shown with black dots, producing a line that is approximately  $-\ell^3/36\theta_{t_{\max}}$ .

and are calculated as

$$A = \iint_R dx dy, \bar{x} = \frac{\iint_R x dx dy}{A}, \bar{y} = \frac{\iint_R y dx dy}{A}, \quad (4)$$

$$\sigma_x^2 = \frac{\iint_R (x - \bar{x})^2 dx dy}{A}, \sigma_y^2 = \frac{\iint_R (y - \bar{y})^2 dx dy}{A}, \quad (5)$$

$$\sigma_{xy} = \frac{\iint_R (x - \bar{x})(y - \bar{y}) dx dy}{A}, \rho_{xy} = \frac{\sigma_{xy}}{\sqrt{\sigma_x^2 \sigma_y^2}}. \quad (6)$$

Using these equations, we can calculate the representa-

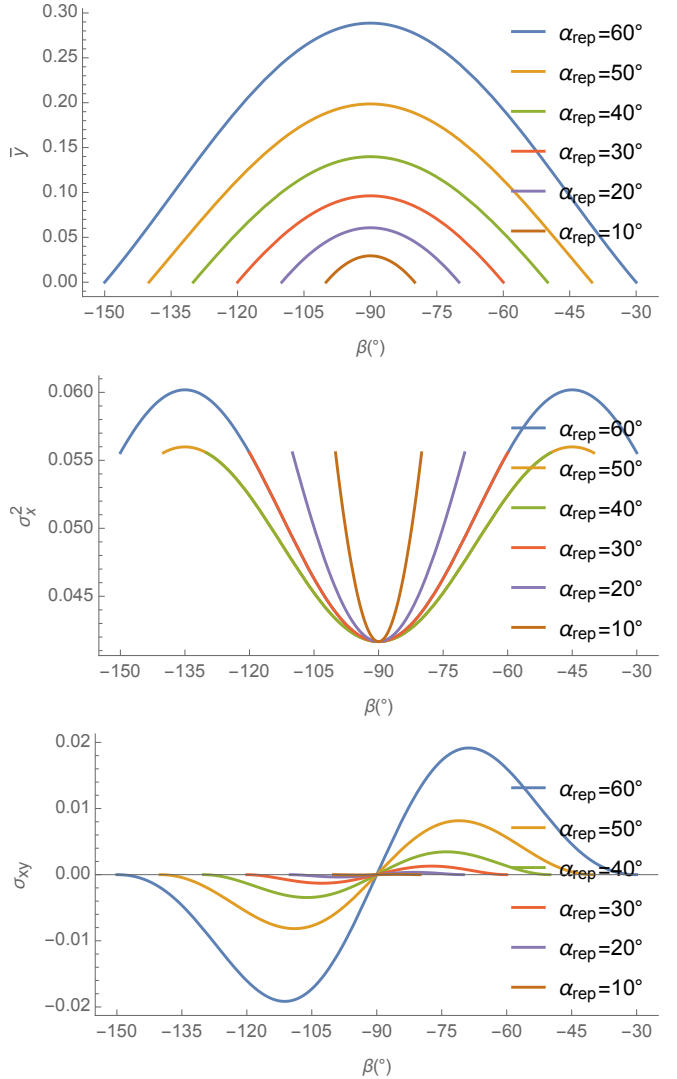


Fig. 4. Each plot shows a statistic of the swarm shape for several angle of repose  $\alpha$  values as a function of the approach angle  $\beta$  with  $\ell = 1$ . Top plot shows the mean  $y$  coordinate  $\bar{y}$ , middle plot shows  $x$ -variance  $\sigma_x^2$ , and bottom plot shows the covariance  $\sigma_{xy}$ .

tive shape statistics as a function of approach angle  $\beta$ , a one degree-of-freedom set. For instance, the area  $A$  of the particles is (1) with  $\theta = \beta + \pi/2$ , and the  $y$ -variance is

$$\sigma_y^2(\alpha, \beta, \ell) = \frac{1}{72} \left( \cot(2\alpha) + \frac{\cos(2\beta)}{\cos(2\alpha)} \right)^2. \quad (7)$$

Representative results are shown in Fig. 4.

#### IV. SHAPE CONTROL USING RIGID BOUNDARIES

Shape control using angle of repose only considers the particles that pile up on the object, but most of the particles pass by. This section instead focuses on shape control of the entire group when all the particles are pushed against rigid boundaries, starting by examining analytically all possible configurations in two canonical configuration spaces, and then examining the effect of boundary layer friction.

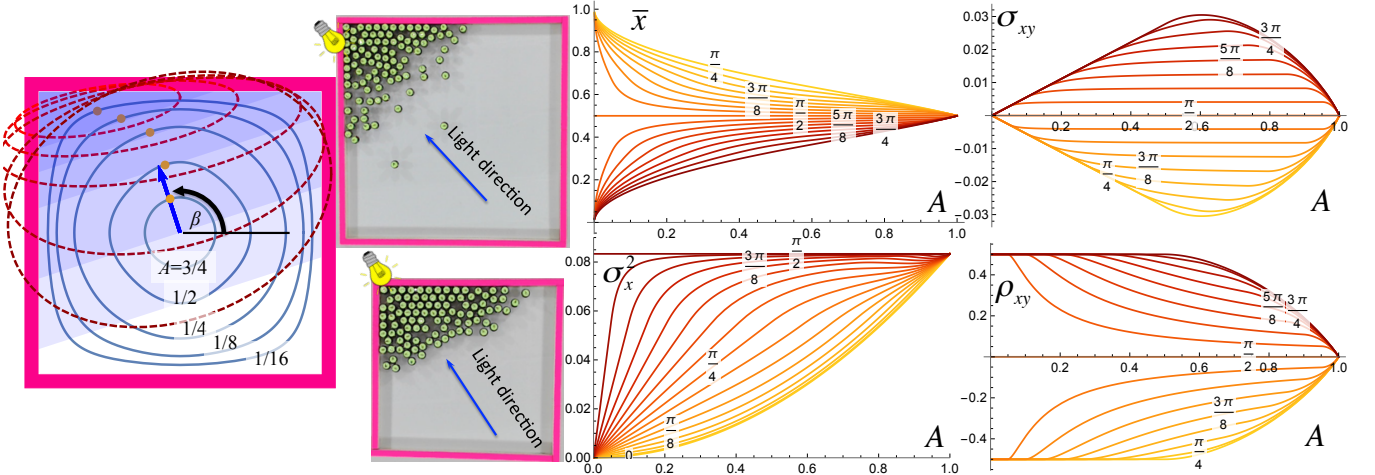


Fig. 5. Pushing the swarm against a square boundary wall allows limited control of the shape of the swarm, as a function of swarm area  $A$  and the commanded movement direction  $\beta$ . Left plot shows locus of possible mean positions for five values of  $A$ . Center shows two corresponding arrangements of kilobots.

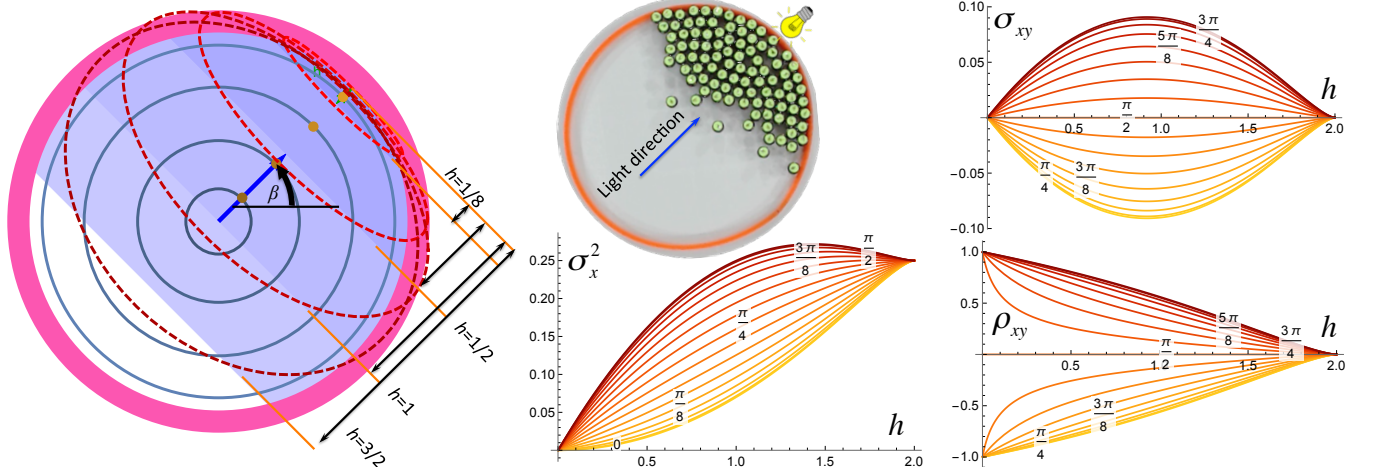


Fig. 6. Pushing the swarm against a circular boundary wall allows limited control of the shape of the swarm, as a function of the fill level  $h$  and the commanded movement direction  $\beta$ . Left plot shows locus of possible mean positions for four values of  $h$ .

### A. Using boundaries: stable configurations of a swarm

One method to control a swarm's shape in a bounded workspace is to simply push in a given direction until the swarm conforms to the boundary. Like fluid settling in a tank, the stable final configuration minimizes potential energy. The set of final configurations are parametrized by a single degree of freedom, the global input angle  $\beta$ .

a) *Square workspace:* We first examine the mean  $(\bar{x}, \bar{y})$ , covariance  $(\sigma_x^2, \sigma_y^2, \sigma_{xy})$ , and correlation  $\rho_{xy}$  of a large swarm of robots as they move inside a square workspace under the influence of a force pulling in the direction  $\beta$ . The swarm is large, but the robots are small in comparison, and together occupy a constant area  $A$ ,  $A \in [0, 1]$ . Under a global input, the swarm moves to a side of the workspace and forms a polygonal shape that minimizes potential energy, as shown in Fig. 5.

The range for the global input angle  $\beta$  is  $[0, 2\pi)$ . In this range, the swarm assumes eight different polygonal shapes. These shapes alternate between triangles and trapezoids

when the area  $A < 1/2$ , and between squares with one corner removed and trapezoids when  $A > 1/2$ .

The region of integration  $R$  is the polygon containing the swarm. For example, if  $A < 1/2$  and the force angle is  $\beta$ , the mean when  $R$  is a triangular region in the lower-left corner is:

$$\bar{x}(A, \beta) = \frac{\int_0^{\sqrt{2A \tan(\beta)}} \left( \int_0^{\cot(\beta)(\sqrt{2A \tan(\beta)} - x)} dy \right) x dx}{A} = \frac{\sqrt{2}}{3} \sqrt{A \tan(\beta)}, \quad (8)$$

$$\bar{y}(A, \beta) = \frac{\int_0^{\sqrt{2A \tan(\beta)}} \left( \int_0^{\cot(\beta)(\sqrt{2A \tan(\beta)} - x)} y dy \right) dx}{A} = \frac{\sqrt{2}}{3} \sqrt{A \cot(\beta)}. \quad (9)$$

The full equations are summarized in Fig. 5. For the full

equations and demonstration code, see [?]. A few highlights are that the correlation is maximized  $\pm 1/2$  when the swarm is in a triangular shape. The covariance of a triangle is always  $\pm(A/18)$ . Variance is minimized in the direction of  $\beta$  and maximized orthogonal to  $\beta$  when the swarm is in a rectangular shape. The range of mean positions are maximized when  $A$  is small.

b) *Circular workspace*: Though rectangular boundaries are common in artificial workspaces, biological workspaces are usually rounded. Similar calculations can be made for a circular workspace. The workspace is a circle centered at  $(0,0)$  with radius 1 and thus area  $\pi$ . For notational simplicity, the swarm is parameterized by the global control input signal  $\beta$  and the fill-level  $h$ . Under a global input, the robot swarm fills the region under a chord with area

$$A(h) = \arccos(1-h) - (1-h)\sqrt{(2-h)h}. \quad (10)$$

For a circular workspace, the locus of mean positions are aligned with  $\beta$  and the mean position is at radius  $r(h)$  from the center which is

$$r(h) = \frac{2(-(h-2)h)^{3/2}}{3\left(\sqrt{-(h-2)h}(h-1) + \arccos(1-h)\right)}. \quad (11)$$

Variance  $\sigma_x^2(\beta, h)$  is maximized at  $\beta = \pi/2 + n\pi$  and  $h \approx 1.43$ , while covariance is maximized at  $\beta = \pi 3/4 + n\pi$  and  $h \approx 0.92$ . For small  $h$  values, correlation approaches  $\pm 1$ . Results are displayed in Fig. 6. For the full equations and demonstration code, see [?].

### B. Using boundaries: friction and boundary layers

Global inputs move a swarm uniformly. Shape control requires breaking this uniform symmetry. A swarm inside an axis-aligned rectangular workspace can reduce variance normal to a wall by simply pushing the swarm into the boundary. If the swarm can flow around each other, pushing the swarm into a boundary produces the limited set of configurations presented in Sec. IV-A. Instead of pushing our robots directly into a wall, the following sections examine an oblique approach using boundaries that generate friction with the robots. These frictional forces are sufficient to break the symmetry caused by uniform inputs. Robots touching a wall have a friction force that opposes movement along the boundary. This causes robots along the boundary to move more slowly than robots in free-space.

Let the control input be a vector force  $\vec{F}$  with magnitude  $F$  and orientation  $\theta$  with respect to a line perpendicular to and into the nearest boundary.  $N$  is the normal or perpendicular force between the robot and the boundary. The force of friction  $F_f$  is nonzero if the robot is in contact with the boundary and  $\sin(\theta) < 0$ . The resulting net force on the robot,  $F_{forward}$ , is aligned with the wall and given by

$$F_{forward} = F \sin(\theta) - F_f,$$

$$\text{where } F_f = \begin{cases} \mu_f N, & \mu_f N < F \sin(\theta) \\ F \sin(\theta), & \text{else} \end{cases} \quad (12)$$

and  $N = F \cos(\theta)$ .

Fig. 7 shows the resultant forces on two robots when one is touching a wall. Though each receives the same inputs, they experience different net forces. For ease of analysis, the following algorithms assume  $\mu_f$  is infinite and robots touching the wall are prevented from sliding along the wall. This means that if one robot is touching the wall and another robot is free, the touching robot will not move when the control input is parallel or into the wall. There are many alternate models of friction that also break control symmetry. Fig. 7c shows fluid flow along a boundary. Fluid in the free-flow region moves uniformly, but flow decreases to zero in the boundary layer [22]. Force in such a system can be calculated as

$$F_{forward}(y) = F - F_f \begin{cases} \frac{h-y}{h}, & y < h \\ 0, & \text{else} \end{cases}. \quad (13)$$

The next section shows how a system in a rectangularly bounded workspace with friction model (12) can arbitrarily position two robots.

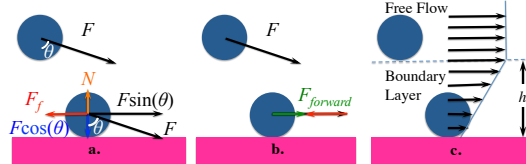


Fig. 7. (a,b) Wall friction reduces the force for going forward  $F_{forward}$  on a robot near a wall, but not for a free robot. (c) velocity of a fluid reduces to zero at the boundary.

### C. Maximizing correlation using wall friction

Assume an obstacle-free, bounded, unit-size, square workspace. As shown in Fig. 5, the maximum correlation occurs when the swarm is pushed in the direction  $\beta = 3\pi/4$ . This correlation as a function of swarm area  $A$  is never larger than  $1/2$ , and the maximum correlation decays to 0 as  $A$  grows to 1. By (6), this maximum correlation is

$$\rho_{xy} = \begin{cases} \frac{1}{2}, & 0 \leq A \leq \frac{1}{2} \\ \frac{3A(2(A-2)A+1)}{4A^3-24A+\sqrt{2}(12A-12)\sqrt{1-A+17}} - 1, & \frac{1}{2} \leq A \leq 1 \end{cases} \quad (14)$$

If friction obeys the linear boundary layer model of (13) with boundary layer thickness  $h$  and maximum friction  $F_f$  equal to the maximum applied force  $F$ , we can generate larger correlations. If the swarm size is smaller than  $\approx 0.43$  and the boundary layer is sufficiently thick we can generate correlations larger than  $1/2$  using boundary friction.

Assume that the swarm is initialized in the lower-left corner, in a rectangle of width  $w$  and height  $A/w$ . Such a rectangular configuration can be accomplished using the variance controllers from [23]. If the swarm is then commanded to move a distance  $L$  to the right, components of the swarm outside the boundary friction layer of height  $h$  move further than components near the boundary. The swarm is contained in a region  $R$  composed of no more than three stacked components: at bottom a parallelogram inclined to the right top, at middle a rectangle, and at top a parallelogram

inclined to the left top. These regions can be defined by the rectangle's left side, bottom, and top:

$$\begin{aligned} r_{\text{left}} &= \min(L, 1 - w), \\ r_{\text{bottom}} &= \min\left(\frac{A}{w}, h \frac{r_{\text{left}}}{L}\right) \text{ and} \\ r_{\text{top}} &= \min\left(\frac{A}{w}, 1 - h \frac{r_{\text{left}}}{L}\right). \end{aligned} \quad (15)$$

If  $\frac{A}{w} \leq r_{\text{top}}$  the top parallelogram has no area. Similarly, if  $r_{\text{top}} \leq r_{\text{bottom}}$  the rectangle has no area. The mean, variance, and correlation are calculated using (4), (5), and (6) over the region  $R$ :

$$\begin{aligned} \iint_R f(x, y) dx dy &= \int_0^{r_{\text{bottom}}} \int_{\frac{L}{h}y}^{\frac{L}{h}y+w} f(x, y) dx dy \quad (16) \\ &+ \int_{r_{\text{bottom}}}^{r_{\text{top}}} \int_{r_{\text{left}}}^{r_{\text{left}}+w} f(x, y) dx dy \\ &+ \int_{r_{\text{top}}}^{\frac{A}{w}} \int_{-\frac{L(y-r_{\text{top}})}{h}+r_{\text{left}}}^{r_{\text{left}}+w-\frac{L(y-r_{\text{top}})}{h}} f(x, y) dx dy. \end{aligned}$$

Given an environment parameterized by  $A$  and  $h$ , efficient correlation control consists of choosing the  $w, L$  pair that generates the desired positive correlation. Negative correlations can be generated by initializing the swarm in the upper left, or lower right.

#### D. Efficient control of correlation

This section examines maximum correlation values as a function of  $w, L$  using (16) from Section IV-C. The maximum correlation using boundary layer friction  $\max_{w, L}(\rho(A, h, w, L))$  can be found by gradient descent, as shown in Fig. 8. For swarms with small area, this method enables generating the full range of correlations  $\pm 1$ . As the swarm area  $A$  increases above  $\approx 0.43$ , the stable configuration method is more effective. Larger boundary layers  $h$  enable more control of correlation. The multimedia attachment shows efficient control of correlation with simulations using the 2D physics engine Box2D [24] and 144 disc-shaped robots with boundary layer model (13).

## V. EXPERIMENTS

### A. Hardware experiment: particle angle of repose

In this section we vary the force and approach angle to shape a swarm with a characteristic angle of repose.

**TODO: Haoran will Explain hardware experiment**

### B. Hardware experiment: kilobot angle of repose

In this section we vary the force and approach angle to shape a swarm of Kilobots [?] with a characteristic angle of repose. Kilobot is a three centimeter low cost robot that has light sensor. In our experiments, these robots were programmed to go toward the brightest light in the room. The experimental setup is shown in Fig. 11. Figure 12 shows angle of repose of the Kilobots with three different angles of the pink rod when the rod has  $0^\circ$ ,  $22.5^\circ$  and  $45^\circ$ . The

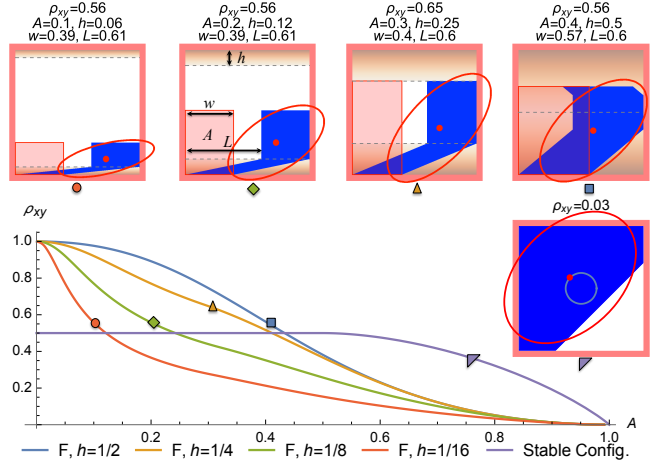


Fig. 8. Analytical results comparing maximum correlation  $\rho_{xy}$  under the boundary layer friction model of (16) with four boundary layer thicknesses  $h$  and the stable triangular configuration (14).

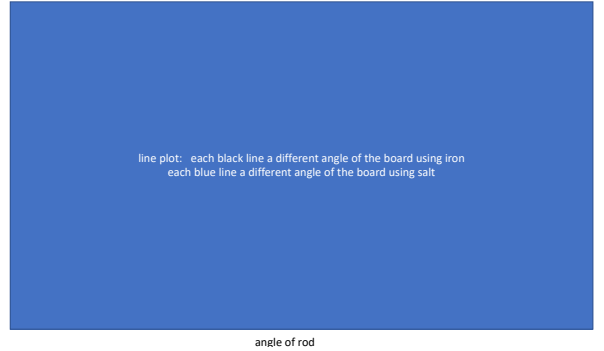


Fig. 9. Experimental data

green lines show the triangle that the robots pile up. The cyan star is the center of mass of the rod, and mean position and variance of the robots are shown with a red star and red ellipse.

### C. Hardware experiment: control of covariance

To demonstrate covariance control, up to 100 kilobots were placed on the workspace and manually steered with lights, using friction with the boundary walls to vary the covariance from  $-4000$  to  $3000 \text{ cm}^2$ . The resulting covariance is plotted in Fig. 13, along with snapshots of the swarm.

## VI. CONCLUSION AND FUTURE WORK

This paper presented techniques for reshaping particles using uniform inputs and non-slip boundary contacts. Hardware experiments illustrated the algorithms in ex vivo and in artificial workspaces.

## REFERENCES

- [1] K. E. Peyer, L. Zhang, and B. J. Nelson, "Bio-inspired magnetic swimming microrobots for biomedical applications," *Nanoscale*, 2013.
- [2] Y. Shirai, A. J. Osgood, Y. Zhao, K. F. Kelly, and J. M. Tour, "Directional control in thermally driven single-molecule nanocars," *Nano Letters*, vol. 5, no. 11, pp. 2330–2334, Feb. 2005.



Fig. 10. Magnified image of salt and iron at angle of repose.

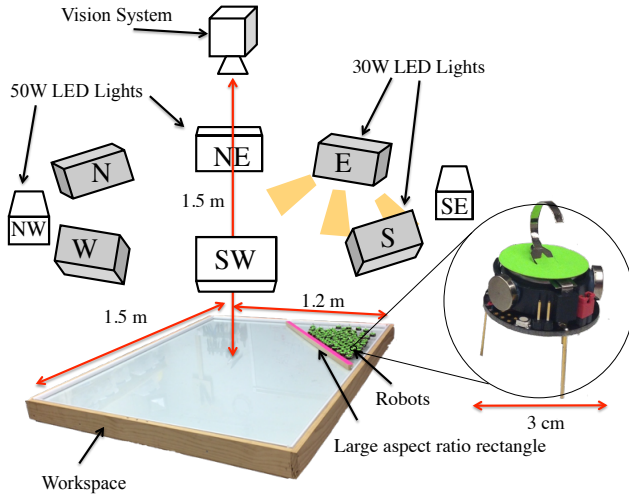


Fig. 11. The platform where we control Kilobots with lights.

- [3] P.-T. Chiang, J. Mielke, J. Godoy, J. M. Guerrero, L. B. Alemany, C. J. Villagómez, A. Saywell, L. Grill, and J. M. Tour, "Toward a light-driven motorized nanocar: Synthesis and initial imaging of single molecules," *ACS Nano*, vol. 6, no. 1, pp. 592–597, Feb. 2011.
- [4] S. Shahrokhi, A. Mahadev, and A. T. Becker, "Algorithms for shaping a particle swarm with a shared input by exploiting non-slip wall contacts," in *Intelligent Robots and Systems (IROS), 2017 IEEE/RSJ International Conference on*, 2017.
- [5] S. Shahrokhi, L. Lin, C. Ertel, M. Wan, and A. T. Becker, "Steering a swarm of particles using global inputs and swarm statistics," *IEEE Transactions on Robotics*, vol. 34, no. 1, pp. 207–219, 2018.
- [6] M. Egerstedt and X. Hu, "Formation constrained multi-agent control," *IEEE Trans. Robotics Automat.*, vol. 17, pp. 947–951, 2001.
- [7] M. A. Hsieh, V. Kumar, and L. Chaimowicz, "Decentralized controllers for shape generation with robotic swarms," *Robotica*, vol. 26, no. 05, pp. 691–701, 2008.

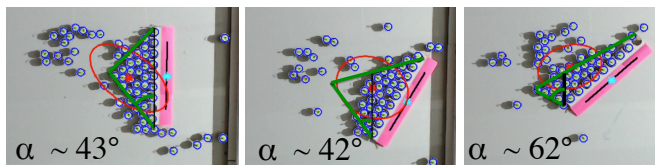


Fig. 12. Angle of repose of Kilobots controlled by light.

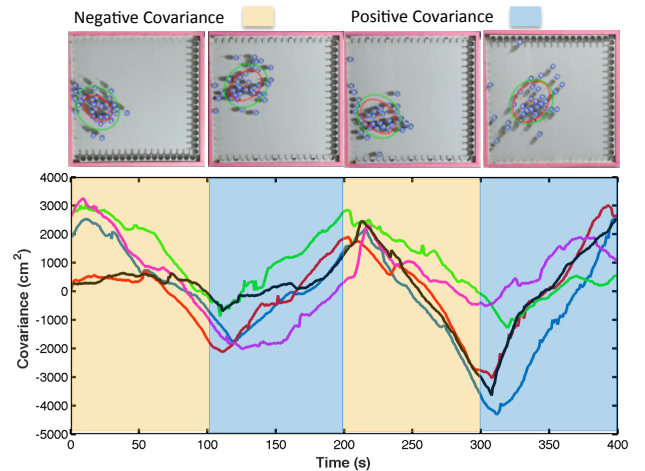


Fig. 13. Hardware demonstration steering  $\approx 50$  kilobot robots to desired covariance. The goal covariance is negative in first 100 seconds and is positive in the next 100 seconds. The actual covariance is shown in different trials. Frames above the plot show output from machine vision system and an overlaid covariance ellipse.

- [8] S. Chowdhury, W. Jing, and D. J. Cappelleri, "Controlling multiple microrobots: recent progress and future challenges," *Journal of Micro-Bio Robotics*, vol. 10, no. 1-4, pp. 1–11, 2015.
- [9] S. Martel, "Magnetotactic bacteria for the manipulation and transport of micro- and nanometer-sized objects," *Micro-and Nanomanipulation Tools*, vol. 13, 2015.
- [10] X. Yan, Q. Zhou, J. Yu, T. Xu, Y. Deng, T. Tang, Q. Feng, L. Bian, Y. Zhang, A. Ferreira, and L. Zhang, "Magnetite nanostructured porous hollow helical microswimmers for targeted delivery," *Advanced Functional Materials*, vol. 25, no. 33, pp. 5333–5342, 2015.
- [11] A. L. Bertozzi, T. Kolokolnikov, H. Sun, D. Uminsky, and J. Von Brecht, "Ring patterns and their bifurcations in a nonlocal model of biological swarms," *Communications in Mathematical Sciences*, vol. 13, no. 4, pp. 955–985, 2015.
- [12] B. R. Donald, C. G. Levey, I. Paprotny, and D. Rus, "Planning and control for microassembly of structures composed of stress-engineered mems microrobots," *The International Journal of Robotics Research*, vol. 32, no. 2, pp. 218–246, 2013. [Online]. Available: <http://ijr.sagepub.com/content/32/2/218.abstract>
- [13] T. Bretl, "Control of many agents using few instructions," in *Proceedings of Robotics: Science and Systems*, Atlanta, GA, USA, June 2007.
- [14] A. Becker, C. Onyuksel, T. Bretl, and J. McLurkin, "Controlling many differential-drive robots with uniform control inputs," *The international journal of Robotics Research*, vol. 33, no. 13, pp. 1626–1644, 2014.
- [15] Z. Nosrati, N. Li, F. Michaud, S. Ranamukhaarachchi, S. Karagiozov, G. Soulez, S. Martel, K. Saatchi, and U. O. Hfeli, "Development of a coflowing device for the size-controlled preparation of magnetic-polymeric microspheres as embolization agents in magnetic resonance navigation technology," *ACS Biomaterials Science & Engineering*, vol. 4, no. 3, pp. 1092–1102, 2018.
- [16] A. Becker, G. Habibi, J. Werfel, M. Rubenstein, and J. McLurkin, "Massive uniform manipulation," in *IEEE International Conference on Intelligent Robots and Systems*, Nov. 2013.
- [17] F. Lamirault and L. E. Kavraki, "Positioning of symmetric and non-symmetric parts using radial and constant fields: Computation of all equilibrium configurations," *International Journal of Robotics Research*, vol. 20, no. 8, pp. 635–659, 2001.
- [18] T. H. Vose, P. Umbanhowar, and K. M. Lynch, "Sliding manipulation of rigid bodies on a controlled 6-dof plate," *The International Journal of Robotics Research*, vol. 31, no. 7, pp. 819–838, 2012.
- [19] S. Salmanipour and E. Diller, "Eight-degrees-of-freedom remote actuation of small magnetic mechanisms," in *IEEE International Conference on Robotics and Automation*, 2018.
- [20] A. Denasi and S. Misra, "Independent and leader follower control for

- two magnetic micro-agents,” *IEEE Robotics and Automation Letters*, vol. 3, no. 1, pp. 218–225, Jan 2018.
- [21] E. Diller, J. Giltinan, G. Z. Lum, Z. Ye, and M. Sitti, “Six-degree-of-freedom magnetic actuation for wireless microrobotics,” *The International Journal of Robotics Research*, vol. 35, no. 1-3, pp. 114–128, 2016.
- [22] P. J. Pritchard, *Fox and McDonald’s Introduction to Fluid Mechanics, 8th Edition*. John Wiley and sons inc., 2011.
- [23] S. Shahrokhi and A. T. Becker, “Stochastic swarm control with global inputs,” in *IEEE/RSJ International Conference on Intelligent Robots and Systems (IROS)*. IEEE, 2015, pp. 421–427.
- [24] E. Catto, “User manual, Box2D: A 2D physics engine for games, <http://www.box2d.org>,” 2010. [Online]. Available: <http://www.box2d.org>